How do ions contribute to brine-hydrophobic hydrocarbon Interfaces? An in silico study

Badizad, Mohammad Hasan; Koleini, Mohammad Mehdi; Hartkamp, Remco; Ayatollahi, Shahab; Ghazanfari, Mohammad Hossein

DOI
10.1016/j.jcis.2020.04.060

Publication date
2020

Document Version
Final published version

Published in
Journal of Colloid and Interface Science

Citation (APA)
Badizad, M. H., Koleini, M. M., Hartkamp, R., Ayatollahi, S., & Ghazanfari, M. H. (2020). How do ions contribute to brine-hydrophobic hydrocarbon Interfaces? An in silico study. *Journal of Colloid and Interface Science*, *575*, 337-346. https://doi.org/10.1016/j.jcis.2020.04.060

Journal of Colloid and Interface Science 575 (2020) 337–346

Contents lists available at ScienceDirect

Journal of Colloid and Interface Science

journal homepage: www.elsevier.com/locate/jcis

How do ions contribute to brine-hydrophobic hydrocarbon Interfaces? An *in silico* study

Mohammad Hasan Badizad [a], Mohammad Mehdi Koleini [b], Remco Hartkamp [c], Shahab Ayatollahi [b,*], Mohammad Hossein Ghazanfari [a]

[a] Department of Chemical and Petroleum Engineering, Sharif University of Technology, Tehran, Iran
[b] Sharif Upstream Petroleum Research Institute (SUPRI), Department of Chemical and Petroleum Engineering, Sharif University of Technology, Tehran, Iran
[c] Process & Energy Department, Faculty of Mechanical, Maritime and Materials Engineering, Delft University of Technology, Leeghwaterstraat 39, 2628CB Delft, the Netherlands

GRAPHICAL ABSTRACT

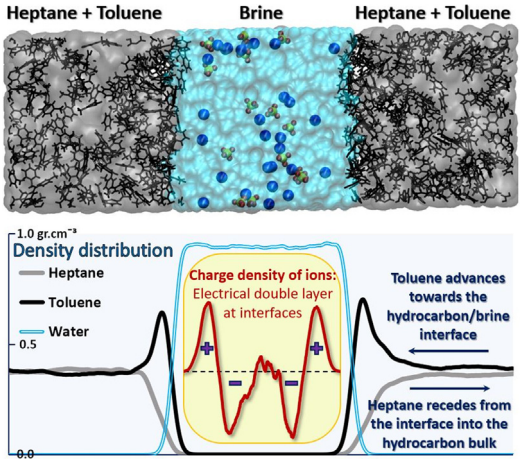

ARTICLE INFO

Article history:
Received 22 November 2019
Revised 14 April 2020
Accepted 15 April 2020
Available online 16 April 2020

Keywords:
Fluid/Fluid Interface
Hydrophobic Aromatic/Aliphatic Hydrocarbons
Non-polar Oil Components
Brine
Electrical double layer
Molecular dynamics simulation

ABSTRACT

Hypothesis: The saltwater-oil interface is of broad implication in geochemistry and petroleum disciplines. To date, the main focus has been on the surface contribution of polar, heavy compounds of crude oil, widely neglecting the role of non-polar hydrocarbons. However, non-polar compounds are expected to contribute to characteristics of oil-brine interfaces.
Methodology: Utilizing molecular dynamics simulation, we aim to characterize ion behavior adjacent to hydrophobic organic phases. Concerning natural environments, NaCl, $CaCl_2$ and Na_2SO_4 electrolytes at low (5 wt%) and high (15 wt%) concentrations were brought in contact with heptane and/or toluene which account for aliphatic and aromatic constituents of typical crude oils, respectively. The reproduced experimental data for interfacial tension, brines density and ions' diffusivities adequately verify our molecular calculations.
Findings: Ions accumulate nearby the intrinsically charge-neutral oil surfaces. A disparate surface-favoring propensity of ions causes the interfacial region to resemble an electrical layer and impose an

* Corresponding author.
E-mail addresses: mohammadhasan.badizad@che.sharif.edu (M.H. Badizad), mmkoleini@che.sharif.edu (M.M. Koleini), shahab@sharif.edu (S. Ayatollahi).

https://doi.org/10.1016/j.jcis.2020.04.060

effective surface charge onto the oil surface. Despite absence of any polar site, the effective surface charge density is hydrocarbon-dependent, with the highest and lowest values observed for toluene and heptane interfaces, respectively. Due to accumulation of toluene molecules nearby the brines, the interfacial characteristics of heptol (toluene-heptane mixture) is comparable to that of the toluene phase.

1. Introduction

Interfaces between hydrophilic and hydrophobic substances are ubiquitous in nature and industry [1,2]. Characterization of saltwater-oil interfaces has been the subject of broad interest in numerous investigations, particularly in the area of improving oil production by low salinity water flooding (LSWF) techniques from subsurface reservoirs [3]. Yet, driving mechanisms and working conditions of LSWF remain elusive [4–7]. All suggested mechanisms, except for wettability alteration, are connected with the fluid-fluid interaction, such as interface viscoelasticity, osmosis, Marangoni effect, emulsification and change of IFT [8]. Evidently, brine-oil interface largely impacts the performance of LSWF process. However, the interfacial contribution of ions at oil-brine interfaces is not fully understood [9], due to the difficulty of probing nanoscopic phenomena at interfaces by direct experimental observation, and because of the complex chemistry of crude oils [10–12]. The discrete character of ions becomes especially important in the tightly confined medium of porous minerals, where continuum theory fails to provide a detailed picture of the ions behavior [13].

As emphasized in recent publications, characterization of the oil-brine interface requires a hierarchical multi-scale approach, with atomic- and field-scale studies as opposite ends of the spectrum [14,15]. From this perspective, atomistic research is of key importance for evaluating the role of certain ions in the narrow space of oil-brine interfaces as well as the thin brine films covering pore surfaces in the underground petroleum resources [4]. For this purpose, molecular dynamics (MD) simulation is a promising tool for gaining knowledge on the physics of substances enclosed within extraordinary thin spaces [16]. MD simulation facilitates developing new theories and improving existing models for surface and bulk properties of fluids by providing insight into the nature and relative strength of inter- and intra-molecular interactions [13]. Leveraging the strength of MD simulation, Underwood et al. studied the salinity dependence of the interfacial tension (IFT) for decane in contact with aqueous NaCl solutions [17]. They pointed out that the interfacial thickness decreases upon increasing salinity, resulting in higher IFTs. Later, Zhao et al. expanded that work by focusing on diluted NaCl solutions and observed a non-monotonic trend of IFT for *n*-decane/brine systems [18]. Khiabani et al. utilized MD simulation to evaluate ion distributions in a $CaCl_2$ solution confined by pure *n*-hexane. The authors reported formation of alternating charged layers close to the hydrocarbon surfaces [19]. By applying dissipative particle dynamics, Remesal et al. obtained IFT values of aqueous (NaCl or $CaCl_2$)/oil (dedecane or benzene) and found calcium to be more surface-active ion than sodium, possibly due to the larger hydration shell of the former [20].

Atomically-resolved understanding of salinity-dependent and ion-specific effects on brine-hydrocarbon interfaces is much needed to advance the field of enhanced oil recovery. To date, the main focus of the experimental, computational and theoretical literature has been on the surface behavior of polar and heavy compounds of crude oil, in an attempt to reveal the effects of salinity on the oil-brine interfaces [21,22]. Although aromatics and aliphatics comprise the major fraction of typical crude oils, there is a paucity of investigation on the interfacial role of those compounds. Recently, Bonto et al. emphasized the importance of non-polar hydrocarbons for regulating the surface charge of water/oil [23]. To address this deficiency, classical MD simulation was utilized in the present work to resolve the interfacial characteristics of NaCl, $CaCl_2$ and Na_2SO_4 solutions in contact with the heptane and/or toluene, as models for the aliphatic and aromatic fraction of typical crude oil. In the remaining of this paper, the simulation methodology is explained in details; then numerical results are verified by comparing against available experimental data for various bulk and interfacial properties. Next, we thoroughly analyze the ion specific effects on the charge distribution near water–oil interfaces. Finally, we conclude by summarizing our main findings.

2. Simulation methodology

2.1. Model construction

The salt effect on the brine-hydrocarbon interface was investigated by considering NaCl, $CaCl_2$ and Na_2SO_4 saline solutions confined by heptane and/or toluene nonpolar phase. Brines of 5 and 15 wt% salinity are considered to, respectively, account for low salinity (LS) brine typical for sea water and high salinity (HS) under-ground water occupying aquifers [24]. We note that controlling the fixed weight percentage of ions in the solution deviates from controlling the molarity of the solution. The latter would be the control parameter of choice for example when directly comparing the behavior of different cations, which is not the focus of this study. The chosen salts are among the main mono- or divalent cations (Na^+, Ca^{2+}) and anions (Cl^-, SO_4^{2-}) constituting natural electrolytes [25]. The hydrocarbon phase was modeled by pure *n*-heptane (C_7H_{16}), pure toluene (C_7H_8) and a 50/50 vol% mixture of both (called heptol). Having equal carbon numbers, heptane and toluene are common surrogates used in experiments to mimic aliphatic and aromatic organic compounds comprising crude oil and fossilized materials in soils [26,27].

The brine-oil system was modeled inside a $4 \times 4 \times 12$ nm^3 orthorhombic box, depicted in Fig. S1 (see Supporting Information), in which water molecules were placed at middle of the cell while being enclosed by two identical stacks of hydrocarbon molecules. The biphasic systems were set up in accordance with the typical thickness of thin brine films found in the oil reservoirs (1–10 nm) and also configurations adopted by previous researchers [4,17–19]. The number of organic molecules in each slab was set to nearly match the reported densities at ambient conditions (toluene: 0.862, *n*-heptane: 0.679, and heptol: 0.775 $g.cm^{-3}$) [28]. Also, the number of ions was chosen to achieve the concentrations mentioned before. In addition to the confined conformations, some complementary cases were built to account for the liquid/vapor equilibrium state (Fig. S2), and the free saline water (Fig. S3), to serve as benchmarks for validating simulation results.

2.2. Simulation details

All simulations were carried out using the LAMMPS package [29]. Periodic boundary conditions were imposed in all directions.

The all-atom OPLS (OPLS-AA) force field was employed to describe inter-atomic potentials of toluene and heptane molecules, with Lennard-Jones (LJ) 12–6 (describing van der Waals, in short vdW) and Coulombic (or electrostatic) relations. Water molecules were modeled by the SPC/E parameterization, the best three-point model for reproducing physical properties of water [30]. The covalent bonds and angles in the rigid water molecules were constrained by the SHAKE algorithm with a tolerance of 1×10^{-5}. Intermolecular interaction of ions was described with a LJ potential and a Coulombic potential, whereas intramolecular interaction of the sulfate ion was described with a harmonic bond and angle potential. The corresponding ion parameters were adopted from [31,32]. The non-bond parameters between dissimilar atoms were derived using the geometric combining rule.

A cut-off radius of 1.9 nm was taken for evaluating short-range LJ and Coulombic forces. This large cut-off is motivated by previous studies which suggested that applying long cut-offs, while obeying the minimum-image convention [33], yields accurate IFTs [34]. The long-range electrostatic interactions were resolved in the reciprocal space by the particle-particle particle-mesh (pppm) scheme with a precision of 1×10^{-5}. The equations of motion were integrated using the velocity-Verlet algorithm with a time step of 1.0 fs. The simulation systems were initially relaxed via the steepest descent approach to remove any potential overlap of particles. They were then equilibrated for 0.5 ns at 296.15 K in the NVT ensemble using a Berendsen thermostat with a coupling constant of 0.1 ps. To relax the system density, the system was equilibrated for an additional 1.5 ns in the NPT ensemble at 296.15 K and 1 atm by applying a Berendsen barostat with a damping constant of 1.0 ps. Convergence was confirmed by monitoring total energy, temperature and volume in the course of the simulation, discussed in Supporting Information, Figs. S4-7.

Next, the simulation was continued for 20 ns in the NP_zAT ensemble, in which the *x-y* surface plane and the normal pressure element (P_{zz}) were fixed, using a Nosé-Hoover thermostat and barostat at preceding temperature and pressure. It is necessary to apply this thermostat for the production run, rather than the Berendsen thermostat, because velocity rescaling algorithms are prone to simulation artifacts [35]. Particle trajectories were extracted every 1 ps for post processing. Thermodynamic and structural properties were obtained by averaging output data over the second half of the simulation time-span together with the pertaining uncertainties calculated by block-averaging method [36].

3. Results and discussion

3.1. Model validation and accuracy evaluation

Prior to exploring the nano-structuring features at brine-oil media, we shall examine the extent to which our simulation setup can reproduce experimentally measurable properties in a bulk system. Because no force field is truly universal, it is essentially a preliminary task to justify the choice of parameterization models and particularly, their compatibility [37]. For this purpose, a stepwise approach was followed to ensure the validity of simulations conducted, while paving a safe way for future use of given ion/water/hydrocarbon models. First, the density of saltwater solutions was obtained at 0.1 MPa and 23 °C, presented in Table 1. The computed densities are in agreement with the empirical values reported in the literature [38]. Further, self-diffusivity of individual ions was estimated according to the popular Einstein's relation [39]. Although the ion force fields that we use were optimized based on thermodynamic properties at infinite dilution, the diffusion coefficients predicted through MD simulation at finite ion concentrations are in reasonable agreement with the corresponding experimental data (Table 2).

Table 1
Density of NaCl, $CaCl_2$ and Na_2SO_4 solutions at LS and HS concentrations obtained from MD simulation at 23 °C. The experimental values reported by Kumar [38] are included in parentheses. Densities are in unit gr.cm^{-3}.

	LS	HS
NaCl	1.0264 ± 0.0005 (1.0360)	1.0784 ± 0.0010 (1.1068)
$CaCl_2$	1.0368 ± 0.0007 (1.0382)	1.1155 ± 0.0007 (1.1243)
Na_2SO_4	1.0477 ± 0.0015 (1.0439)	1.1451 ± 0.0023 (1.1346)

To this stage, we have verified the ability of the chosen ion force fields to reproduce two relevant experimental bulk properties. Now, we take a step ahead to validate the utility of the OPLS-AA force field for modelling the toluene and heptane molecules in conjunction with the ions and the water. For this validation, the IFT of different hydrocarbon-saltwater interfaces were obtained through the Irving–Kirkwood approach [40]. IFTs reproduced through our MD simulations, as presented in Table 3, are consistent with the respective empirical data. In sum, various benchmarks against experimental data (density, self-diffusivity and IFT) demonstrate the compatibility of the selected set of force fields for the ions, water and hydrocarbons. The slight salinity-dependence of oil-brine's IFTs, reported in Table 3, arises from the absence of surface active (functionalized) constituents in the oil phase considered here. It should be noted that the variation of oil-brine's IFT is not the focus of this study; it merely serves for a benchmarking purpose. In the current work, we primarily aim to resolve the interaction of ions and aliphatic/aromatic compounds at atomic-resolution. To the authors' knowledge, the utility of potentials adopted for calcium and sulfate ions have not previously been explored in the context of electrolyte-oil interfaces.

3.2. Concentration and charge density distribution

To begin our analysis, the distribution of constituting compounds along the direction perpendicular to the interfaces, i.e., z-axis, was analyzed by counting the presence of these compounds in parallel bins of 0.1 Å thickness. The same practice was followed to obtain the charge density profile, altogether displayed in Fig. 1 (heptol/$CaCl_2$ solution), Figs. S8-9 (heptol/NaCl or Na_2SO_4 solution) and Figs. S10-12 (toluene or heptane/brine). Two interstitial layers, termed interfaces, are seen at the junction of water and hydrocarbon density profiles where all kinds of components are present. These interfaces separate the bulk of encompassing aqueous and hydrocarbon phases, each with densities equivalent to their pure state at atmospheric condition. By this consideration, the inhomogeneous multicomponent system could be essentially divided into five parts, namely, two interfaces, two bulk hydrocarbons and an intervening brine, as sketched in Fig. S14.

Remarkable in each heptol-brine system, the density profile of toluene exhibits a maximum near the interfaces, indicating accumulation of toluene molecules nearby the water phase. This accumulation is also visible in the final snapshots of heptol-brines, Figs. 1 and S8-9. In this circumstance, the heptol density at the bulk region (confined roughly within 0 nm < z < ~4 nm and ~ 8-nm < z < 12 nm) is slightly lower than the value expected for the pure state, 0.753 against 0.775 g.cm^{-3}, respectively. This discrepancy is caused by the partial depletion of organic bulk phase by toluene due to its loading adjacent to the aqueous solution. It seems that toluene effectively plays the role of a surfactant-like component in the presence of heptane, whereas it is dormant at the pure state, for example compare Figs. 1 and S10. As an incentive to the current study, Kunieda et al. pointed out the enhanced concentration of benzene at the interface of a light oil and water

Table 2
Self-diffusion coefficient of cations and anions constituting binary electrolyte solutions of NaCl, $CaCl_2$ and Na_2SO_4 at ambient conditions. The experimental data are presented in parentheses. All values are in unit 10^{-9} $m^2.s^{-1}$.

	LS		HS	
	Cation	Anion	Cation	Anion
NaCl	1.152 (1.236[a], 1.247[b])	1.306 (1.806[a])	0.839 (1.088[a], 1.061[b])	1.208 (1.532[a,*])
$CaCl_2$	0.685 (0.709[a])	1.366 (1.665[a])	0.692 (0.560[a])	1.244 (1.420[a])
Na_2SO_4	1.394 (1.082[c])	0.579 (0.859[c])	0.537 (0.790[c,*])	0.461 (0.570[c,*])

[a] Reported by Mills and Lobo [41].
[b] Adopted from Mills [42].
[c] Presented by Weingiirtner et al. [43].
[*] Interpolated value.

Table 3
IFT of Hydrocarbon (toluene, heptane or heptol)/brine interphases predicted by MD simulation at 23 °C. Values inserted in parentheses are results of experiment presented by Kumar [38]. Surface tension, in second column, refers to the liquid/vapor interface of hydrocarbon.

	Surface tension (mN/m)	Interfacial tension (mN/m)						
		Pure water	NaCl		$CaCl_2$		Na_2SO_4	
			LS	*HS*	*LS*	*HS*	*LS*	*HS*
Toluene	26.6 ± 0.2(28.3)	36.7 ± 0.7(36.1)	36.6 ± 0.4(36.36)	39.1 ± 0.6(39.40)	38.0 ± 0.7(35.30)	42.1 ± 0.5(37.73)	37.8 ± 0.3(35.01)	40.7 ± 0.6(36.95)
Heptane	17.0 ± 0.4(19.8)	51.9 ± 0.4(50.1)	50.8 ± 0.6(50.95)	53.5 ± 0.3(53.35)	53.9 ± 0.8(50.46)	56.1 ± 0.9(NA)[a]	51.5 ± 0.6(49.83)	52.1 ± 0.7(50.88)
Heptol	23.5± 0.2(22.36)	40.2 ± 0.5(40.3)	41.5 ± 0.8(39.44)	44.1 ± 0.5(42.95)	42.0 ± 0.6(39.85)	45.2 ± 0.5(42.47)	41.3 ± 0.5(40.53)	42.6 ± 0.5(41.40)

[a] Experimental value is not available.

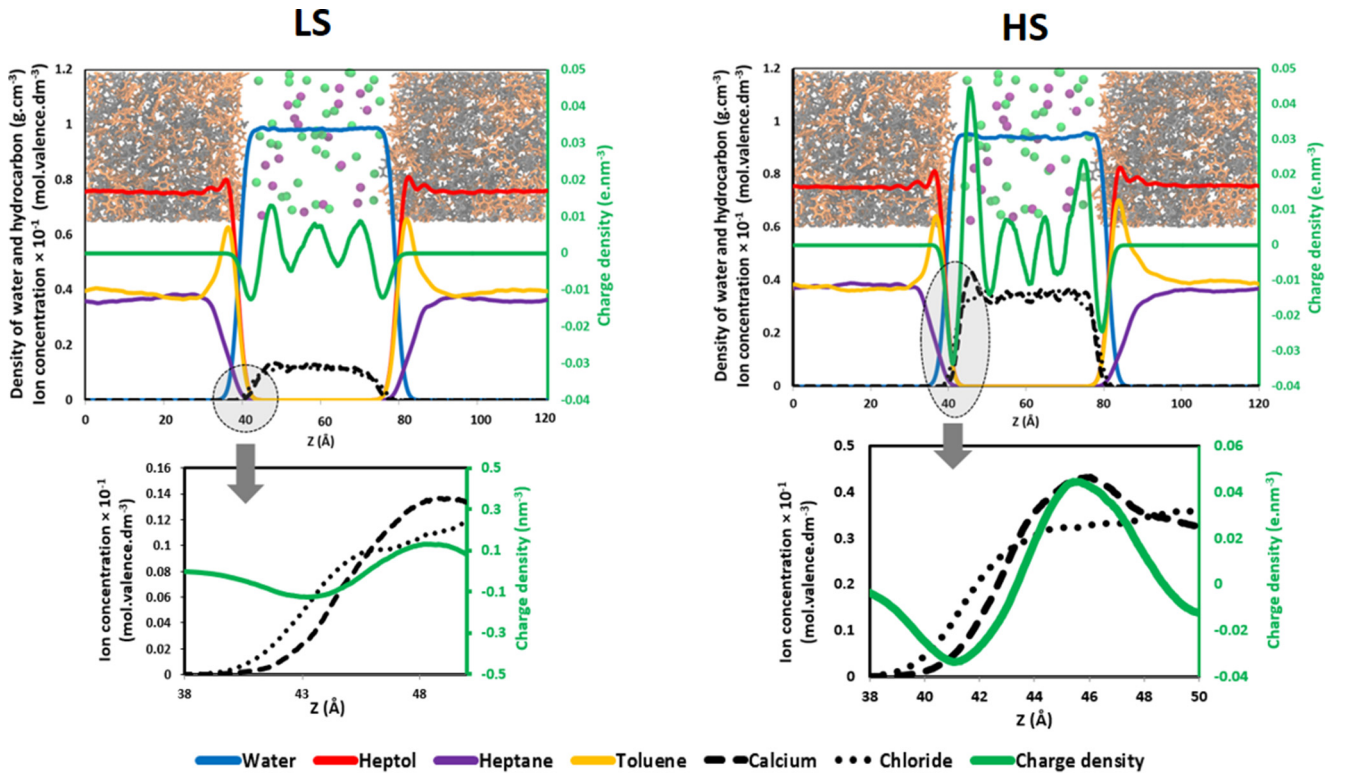

Fig. 1. Distribution profiles of water, toluene, heptane, chloride and calcium across the heptol-brine biphasic system at low (left-hand panel) and high (right-hand panel) salinity state of $CaCl_2$. The embedded snapshots are taken at last frame, with color-code toluene: orange, heptane: gray, calcium: green, and chloride: purple. The water molecules are hidden for clarity. The ion concentration is presented in molar units multiplied by ion's valence. (For interpretation of the references to color in this figure legend, the reader is referred to the web version of this article.)

[44]. They argued that the self-accumulation of aromatics at the oil–water interface is driven by their greater surface affinity than paraffinic components. This much-less-understood virtue of aromatics is well mirrored microscopically in the lower IFT of toluene-water (36.1 $mN.m^{-1}$) compared to heptane-water (50.1 $mN.m^{-1}$). Also, the IFT of heptol, 40.3 $mN.m^{-1}$, is lower than the algebraic average of those of heptane and toluene, 43.1 $mN.m^{-1}$. Altogether, we infer the non-ideality of the heptol phase, so that its micro- and macroscopic properties cannot be interpolated through a simple linear mixing rule. This fact was also pointed

out by Kunieda et al., who observed that the heptol's surface tension and density did not follow a linear relationship against the compounds' mole fraction [45]. The non-ideality associated with the heptol mixture hints us to the complicacy in modelling surface and thermodynamic properties of crude oil, which is a complex mixture of numerous aliphatic, aromatic and polar compounds.

The charge density distributions, shown in Figs. 1 and S8-12, compare the likelihood of cations and anions to occur nearby the hydrocarbon phases. At first glance, we notice an electrical double layer (EDL) consisting of two alternating charged layers immediately next to the hydrophobic surface. Although charge density profiles appear irregular, an EDL is clearly distinct adjacent to each confining oil phase. This is because the charge density attenuates just beyond the interfaces toward the brine center. Depending on the dissolved electrolyte, either negatively (for NaCl and $CaCl_2$ solutions) or positively (for Na_2SO_4) charged layer appears closer to the organic medium. Note that charge density profiles shown in Fig. 1 were derived by valence-weighted averaging of ion distribution profiles in corresponding panels. Due to statistical virtue of atomistic problems and also the finite number of ions in consideration, the ions distribution and consequently, the charge density profiles are not perfectly symmetric. Considering this un-even distribution, all interface-related analyses were performed by averaging quantities over both oil–water interfaces.

To ensure that our analyses are not subject to finite-size effect, a complementary simulation was carried out with a thicker (8 nm) LS solution of $CaCl_2$ confined by heptol mixtures, shown in Fig. S13. The general trends of charge density and species distribution in this larger system agree with the data shown in Fig. 1. Furthermore, the IFT of the larger heptol-$CaCl_2$ solution was found to be consistent with the corresponding value for the smaller system, reported in Table 3. Altogether, we conclude that our brine-oil systems are large enough to avoid plausible interaction between the interfaces.

Inherent to the charge-neutrality and the absence of any polar functionality of the hydrocarbon phases considered, there is no apparent adsorption site for selective capturing of ions. With this in mind, we should interpret the EDLs by thinking of the different affinity of the anions and cations for approaching the organic surface. In comparison to typical mineral-brine systems, hydrocarbon phases considered here are weakly ion favoring. For instance, Koleini et al. reported a charge density of a calcite-brine system at a similar salinity, which was three orders of magnitude greater than the value presented for LS NaCl in Fig. S8 [46]. According to the magnified pictures taken at the marked interfaces, one will find out a biased distribution of cations and anions in $CaCl_2$ and NaCl solutions adjacent to the oil phases. In the case of Na_2SO_4 brine, Fig. S9, the cations and anions do not penetrate equally into the hydrocarbon interface, with sodium appearing ~0.2 nm ahead of sulfate.

Particular to the concentrated NaCl and Na_2SO_4 solutions, a dip is observed in the water density profiles in the center of the brine phases, Figs. S8-9. At the same place, there is a hump-like distribution of ionic concentration. The simulation snapshots shown in Figs. S8-9, demonstrate the formation of ionic aggregates in concentrated NaCl and Na_2SO_4 solutions. One should distinguish such ionic clusters from the solid crystals forming upon precipitation, because the salinities considered here are sufficiently below the saturation concentration of the electrolytes, NaCl: 35.89, $CaCl_2$: 74.5, and Na_2SO_4: 19.5 wt% at 20 °C [47].

Increasing the salinity level generally intensifies the EDL layers [48]. This effect is much more pronounced for $CaCl_2$ solutions and to lesser extent for NaCl. In contrast, the interfacial ion accumulation is attenuated in concentrated Na_2SO_4 brine, shown in Fig. S9. This peculiarity is ascribed to the lower number of free ions caused by drastic complexion at concentrated Na_2SO_4 solution. In this respect, Sherman and Collings stated that the effective ionic strength at a high salinity level may not be as much as the expected value for an otherwise fully dissociated salt [49].

3.3. Interface thickness

The degree of miscibility of two fluids could be evaluated in terms of the thickness of their delimiting interface. From a physical perspective, the interfacial width is a qualitative measure for the relative strength of interactions between molecules of two meeting phases compared to self-interactions inside each medium [50]. The interfacial width, Δ, in each brine-hydrocarbon system was obtained through fitting density profiles of oil and water, ρ_o and ρ_w, to the following expression [17]:

$$\rho(z) = \frac{\rho_o + \rho_w}{2} + \frac{\rho_o - \rho_w}{2}\tanh\left(\frac{z - z_0}{\sqrt{2}\Delta}\right) \quad (1)$$

with z_0 denoting the interface location along the z-axis, as marked in Fig. S14.

It is a matter of interest to evaluate the dependence of the interfacial thickness on the salinity and also the identity of confining organic molecules, presented for $CaCl_2$ in Fig. 2 and for other solutions in Fig. S15. First, the interfacial width of the de-ionized water (DW)-hydrocarbon drops upon introducing salts into the system. Further, it slightly decreases, on average 0.2–0.3 Å, upon increasing the salinity from LS to HS in all solutions. This behavior signifies the diminished miscibility of brine and hydrocarbons upon increasing the salt concentration, well reflected by the higher IFT of HS solutions than LS ones (see Table 3). Similarly, the decrease in interface thickness was also pointed out in prior studies for salt solution-vapor systems [51]. In concentrated solutions, the strong electrostatic forces induced by ions encourages polar water molecules to interact preferably with the interior hydrophilic bulk, rather than meeting the hydrophobic compounds at the interface. In light of this conceptual explanation, prior studies pointed out that the interface width of both vapor/liquid and liquid/liquid systems is inversely proportional to the amount of dissolved salt [17,18].

It should be emphasized that the interface thickness strongly depends on the identity of confining hydrocarbons, with the widest and narrowest ones detected for the toluene and heptane phases, respectively. Unsurprisingly, the IFT (Table 3) correlates with the interface thickness, which in turn is directly connected to the aro-

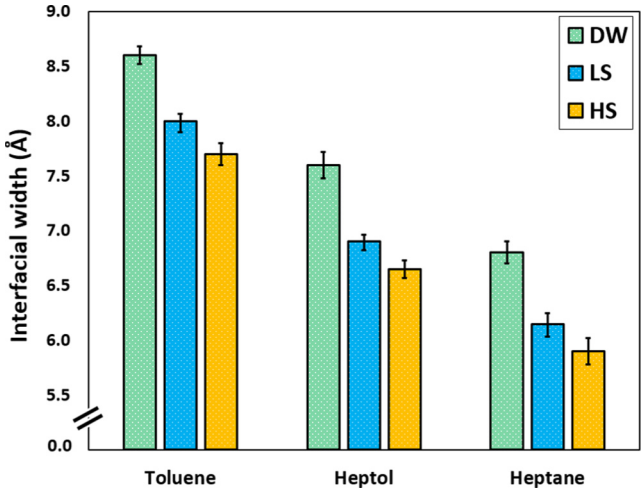

Fig. 2. Interfacial thickness of toluene-, heptane- and heptol-brine systems containing $CaCl_2$ low (LS) and high (HS) salinities. The interfacial width of hydrocarbon-deionized water (DW) are shown for comparison.

matic content of the hydrocarbon phase. One may generally deduce that toluene, as a representative of aromatics in crude oil, exhibits larger surface activity with water, compared to the aliphatic compounds, herein modeled by heptane.

3.4. Interfacial concentration of ions

To further examine ions' localization near the hydrophobic surface, interfacial ion concentrations were computed, for $CaCl_2$ in Fig. 3 and for other solutions in Fig. S16. Interfacial concentration of a certain ion type was acquired by counting and averaging number of ions entered into the interface regions (sketched in Fig. S14) throughout the simulation. To compare surface charge densities, the concentration difference of cations and anions at the oil-water surface are marked in the corresponding figures.

At first glance, one notices the ions' concentrations at the interfaces are lower than the bulk values set by adding salt to the aqueous solutions. This translates to a preference of the ions to stay in the interior of the bulk brine, which has been historically explained under a continuum picture in the literature [52]. In both $CaCl_2$ and NaCl, chloride is more populated at interfaces than its counterions, Ca^{2+} or Na^+, rendering a negatively charged layer near the oil phases. This effect is stronger in concentrated solutions, though both cations (Ca^{2+} and Na^+) and anions (Cl^-) are of higher surface contribution at high salinity level. Particular to Na_2SO_4 electrolyte, we notice the diminished potential of Na^+ and SO_4^{2-} ions for meeting the interface at the HS state. Noteworthy, the surface charge density is weakened by increasing the Na_2SO_4 concentration (Fig. S16b). Such apparently surface-fearing inclination is undoubtedly explained by the formation of interior ionic aggregates, which severely holds ions in the bulk of concentrated solution. The charge density profiles (Fig. S9) show a positively charged layer formed at the interface of the hydrocarbon-Na_2SO_4 solution. It seems that the sodium cations penetrate somewhat further into the interfacial region, owing to the smaller cation size compared to the sulfate anion.

Analogous to the hydrocarbon-brine systems considered here, ion segregation also happens in case of brine-vapor interface [52]. Greater surface propensity of anions (herein Cl^-) than alkali cations has been attributed to their relative abilities for structuring water molecules [53]. Anions and cations are typically classified as kosmotrope (order-making) or chaotrope (order-breaking) [54]. In this notion, anions tend to disturb hydrogen bonding of surrounding water molecules; hence, they are likely to approach the interface. On the contrary, cations can better organize their peripheral water molecules and as a result, it is more favorable to stay in the interior of the bulk solution [55].

In all saline solutions, the toluene interface exhibits greatest capability for ions accommodation. This could be partly explained by the thicker interface of toluene-brine systems, already notified in Figs. 2 and S15. In the same way, the ion concentration correlates with the identity of the touching hydrocarbon in the order: toluene > heptol > heptane. Broadly speaking, we may hypothesize that aromatic components enhance the ionic concentration nearby a non-polar hydrocarbon. The same ascending trend holds for the surface charge density of NaCl and Na_2SO_4 (Fig. S16). Exceptionally, the concentrated $CaCl_2$ solution shows greater surface charge density at the heptane-water interface (Fig. 3). This point will be analyzed by further evidence in following.

3.5. Residence time

Residence time is a useful quantity for evaluating the kinetics of ion capturing by an interface [39]. It serves as a measure to assess the rate of ion swapping between bulk and interface regions. Suppose $N(t_0)$ ions came into an interface at time t_0 and $N(t_0, t_0 + t)$ ions retained in that place until instant $t + t_0$. By this definition, the residence time over T initial steps is defined as [56]:

$$\tau_R = \lim_{t^*\to\infty} \int_0^{t^*} \frac{1}{T} \sum_{t_0=1}^{T} \frac{N(t_0,\ t_0+t)}{N(t_0)} dt \qquad (2)$$

The residence times calculated for each ion type are presented for $CaCl_2$ in Fig. 4 and for other brines in Fig. S16. Unlike the typical crude oil-brine, there is no potential site (charged or strong polar group) in hydrocarbon phases for capturing ions. Therefore, as implied by residence times in Fig. 4, ions are loosely held nearby the hydrocarbon-water surfaces, unwilling to stay within the interface regions.

By increasing the salinity, ions comprising $CaCl_2$ and NaCl electrolytes tend to stay longer at the interface. In contrast, the salinity level adversely impacts the residence time of Na_2SO_4 ions, despite the decreased diffusivity (Table 2). Noteworthy, the salt-dependence of the residence time is analogous to that already observed for the interfacial concentrations of ions, Fig. 3. Similarly, the residence time of ions at the interface depends on the composition of the confining hydrocarbon. Motivated by the longest residence times belonging to the toluene-brine interphases, one may speculate that aromatic compounds promote the ions' willingness for remaining at a hydrocarbon surface.

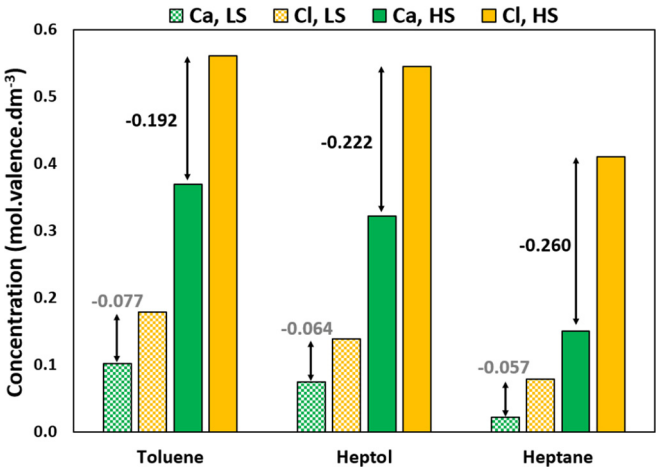

Fig. 3. Interfacial concentration of calcium and chloride in $CaCl_2$ electrolyte contacting hydrocarbon media at low (LS) and high (HS) salinity levels. The charge densities (difference in concentrations of anion and cation) are marked by the arrows.

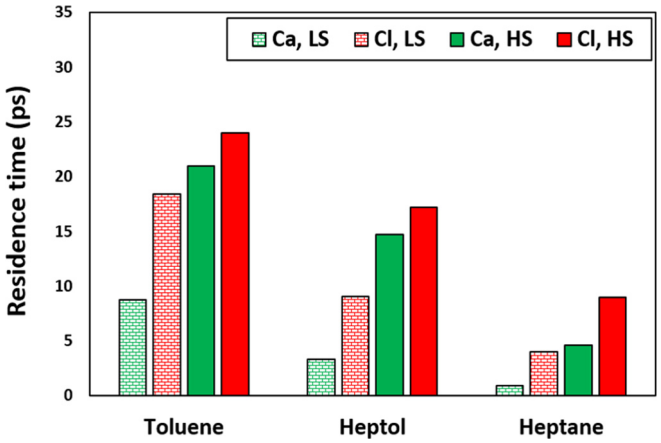

Fig. 4. Residence time of ions for staying at the interface of hydrocarbons- $CaCl_2$ solution at LS and HS conditions.

3.6. Interaction energy of ion-hydrocarbon

Thus far, we realized the existence of an ion-specific effect, which discriminates the propensity of ions for entering into the hydrocarbon interface. To scrutinize the ion-specific segregation at interface regions, the mean potential energy felt by the ions due to interacting, both through vdW and Coulombic forces, with the organic molecules in the confining hydrocarbon phases was calculated for $CaCl_2$, Fig. 5, and for other electrolytes, Fig. S18. The data show that the confining hydrocarbons exert attractive force on chloride and sulfate ions but repel sodium and calcium, indicated by the negative and positive interaction potentials, respectively. These interactions could enhance or weaken the chance of ions to access the interface zone. Despite surface-favoring interactions between sulfates and hydrocarbon phases, Fig. S18, the sodium ions are more prevalent at the interface, as previously inferred by the positively charged interface of Na_2SO_4, Fig. S9. The surface paucity of SO_4^{2-} underlines the paramount influence of the solvation in the bulk aqueous solution, which strongly offsets the surface-favoring interactions arisen by contacting organic phases.

Electrostatic (Coulombic) force is naturally the main kind of interaction felt by ions. Its relative contribution to each corresponding total interaction energy is presented in Figs. 5 and S18. Due to having an imperfect quadruple moment [57,58], the pure toluene phase exerts the strongest electrostatic and thus, the most powerful interaction energy on ions. Interestingly, the interaction energy belonging to ions-heptol are comparable to that arisen by toluene, both prominently greater than that of ion-heptane. It could be attributed to the accumulation of toluene molecules adjacent the aqueous solution, as corroborated by density profiles, Fig. 1. This implies the major ion-hydrocarbon interactions in brine-heptol system is induced by surface-loaded toluene molecules. To summarize, the magnitude of interaction energy per each ion is related to the essence of contacting hydrocarbon, following the order: toluene > heptol > heptane. This sequence recalls the dependence of ions interfacial concentrations on the hydrocarbon identity, discussed in section 3.4.

3.7. Radial distribution function

Radial distribution function (RDF) was employed for revealing the spatial structuring at the oil interface. To this goal, the RDF profile was obtained for water-hydrocarbon and ion-hydrocarbon (with respect to the center of toluene ring and central carbon of *n*-heptane), shown for $CaCl_2$ in Fig. 6 (for NaCl and Na_2SO_4 refer to Fig. S19).

Two dominant peaks are seen in the RDF of water-toluene, the inset in Fig. 6 (also see Figs. S20-21 for the whole set of profiles), which signifies water structuring at toluene and heptol interfaces. In agreement with former studies, Kunieda et al. figured out a similar RDF profile for water-benzene [44]. The appearance of such structuring was ascribed to the tendency of water molecules for establishing a weak H-bond interaction with aromatic compounds. Through this scheme, as sketched in Fig. S20, a water molecule stays at the interface by orienting its hydrogen atoms towards the toluene ring [44]. Following previous investigations [58–60], the first peak at around 3.2 Å in the water-toluene RDF, Fig. S20, belongs to axial H-bonding and second peak at 5.2 Å (amounts to twice length of oxygen-hydrogen bond) is due to self-structuring of farther water molecules. To further assess the impact of toluene-water interaction, an additional simulation was performed in which pure water was enclosed by heptol mixtures, following the protocol explained earlier in section 2. The resulting density profiles, shown in Fig. S22, are identical to those obtained for saline solutions confined by heptol phase, Figs. 1 and S8-9. Thus, toluene accumulation at the brine interfaces is driven by affinity for establishing weak H-bonds with contacting water molecules. Unlike toluene, the broad hump in the RDF of water-heptane, inset of Fig. 6b, implies a fairly negligible water structuring at the interface.

The significant peaks in RDF profiles of Cl^--toluene, Figs. 6a and S19a-b, indicate that the chloride anions are prone to localize around the toluene molecules at the hydrocarbon interface. It seems that localization of any chloride near the toluene ring is mediated by at least one water molecule, as inferred by the coincidence of the peak of Cl^--toluene RDF and the second peak of water-toluene, Fig. 6. Furthermore, the significant peak in the RDF profile

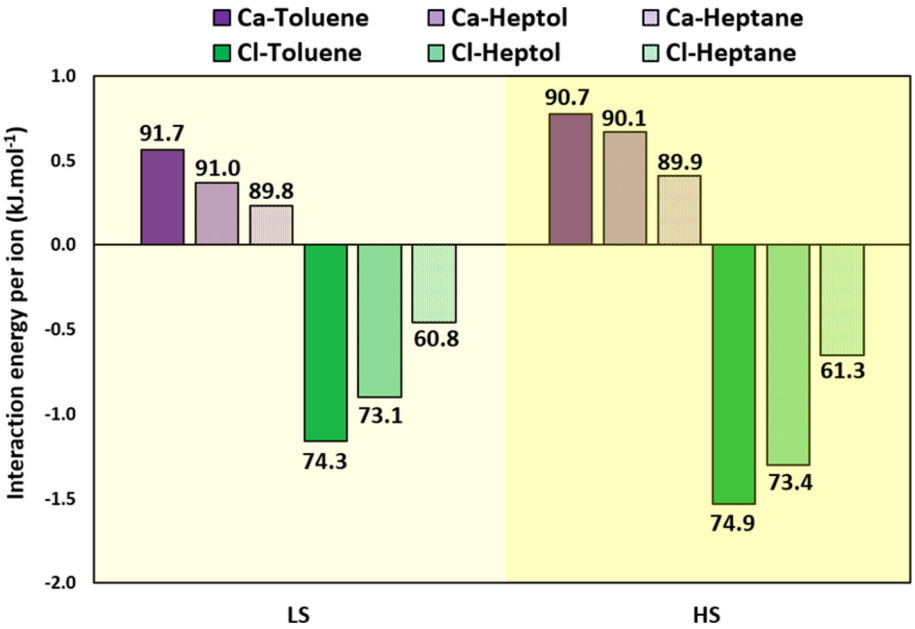

Fig. 5. The average potential energy felt by each ion type due to interacting with hydrocarbon molecules in the confining organic phases at low (LS) and high (HS) salinity states. The values written below and above the bars denote the relative contribution (i.e., percentage) of due to electrostatic interactions.

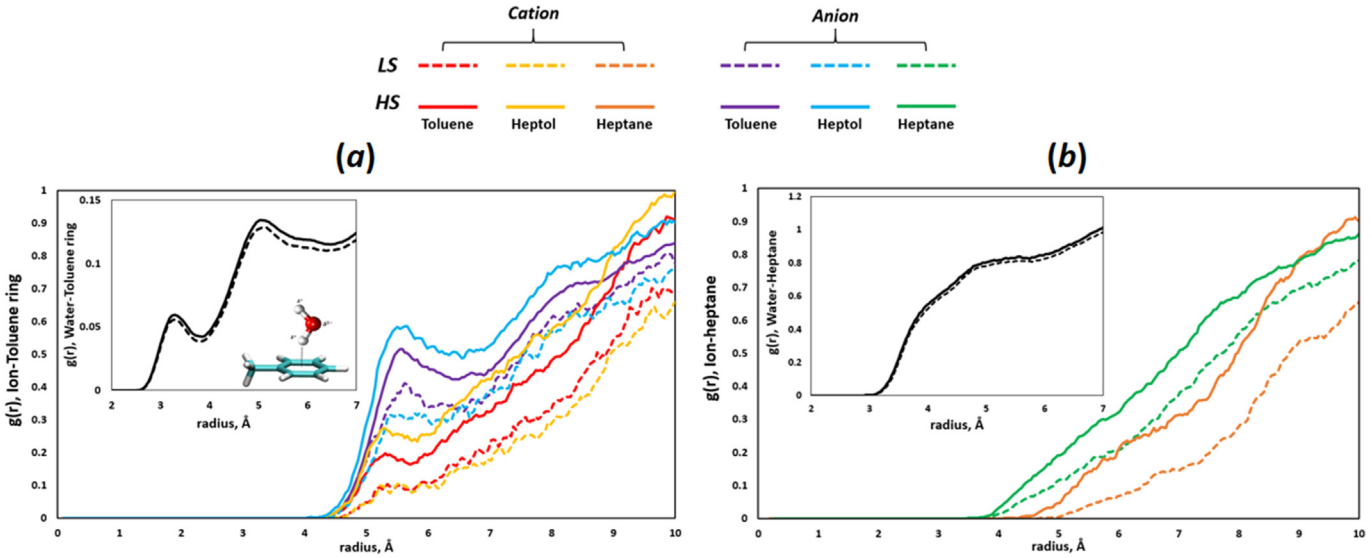

Fig. 6. Ion-toluene and ion–heptane RDF profiles at the interface of $CaCl_2$ solution and different hydrocarbons: (*a*) toluene or heptol, and (*b*) heptane phase. Insets show RDF of water structuring around the toluene ring and central carbon of heptane at low (dashed line) and high (solid line) salinity states.

of $CaCl_2$ solution indicates the presence of calcium ions around the toluene molecules. This might be due to the fairly strong hydration shell of Ca^{2+} [61,62], which ties that ion to water molecules covering the surface of toluene molecules at the interface. The stronger interface affinity of Ca^{2+} than Na^+ could also be interpreted on the basis of cation-π interaction, i.e., the favoring association of cations with bare plane of aromatic rings [57]. It has been demonstrated by first principle computations that divalent cations are of greater propensity to aromatic entities than monovalents [63–66]. Although hydration of ions and toluene drastically suppresses the cation-π effect, it still seems to promote Ca^{2+} access to the interface region. The stronger aromatic-loving tendency of Ca^{2+} is also noticed in the lower interfacial charge density of toluene-brine compared to the heptane-brine system, shown in Fig. 3.

4. Conclusions

In many geo- and petro-chemical processes, biphasic oil-brine systems are subjected to drastic salinity alteration; for example, improving oil production by injecting sea water into the subsurface reservoirs [67]. Characteristics of the oil-saltwater interface have been traditionally investigated by focusing on the role of polar (functionalized) compounds of the crude oil [9,11,15,49], whereas the impact of aromatic and aliphatic species (major non-polar constituents of typical crude oils) has been largely neglected in former investigations.

In this study, classical atomistic simulation was employed to provide a molecular-level view on the behavior of ions within the contact region of various hydrocarbon-brine systems. We focused specifically on the non-polar fraction of crude oil (aliphatic and aromatic) to analyze their interplay with ions in an electrolyte solution. To this end, toluene, heptane and their mixture, called heptol, were considered in a biphasic system encompassing dilute (5 wt%) and concentrated (15 wt%) NaCl, $CaCl_2$ and Na_2SO_4 solutions. The reliability of simulation outputs was verified by benchmarking salt solutions densities, ions' diffusivities and IFTs of hydrocarbon-brine at varying salinities against experimental data.

Ions accumulate at the intrinsically charge-neutral hydrocarbon-brine interface, despite the fact that the non-polar hydrocarbons lack any privileged site, like functional group, for ion accumulation. A disparate propensity of anions and cations for approaching the organic phases results in alternating positively and negatively charged fluid layers, resembling an electrical double layer (EDL). Due to an excess of Cl^- ions at the interface, hydrocarbon surfaces seem as if they are positively charged when exposed to NaCl and $CaCl_2$ solutions, whereas they look negatively charged by surface paucity of sulfate anions in Na_2SO_4 brine. This indicates that unlike typical crude oils, the strength, and even the sign, of charged layers nearby non-polar hydrocarbons are regulated by the composition of contacting electrolytes. The interfacial charge density is regulated by the composition of contacting hydrocarbons, following the general trend toluene > heptol > heptane. Notably, the heptol phase exhibits interface characteristics closer to that of pure toluene, because of toluene accumulation at the aqueous interface. Motivated by results in this work, we shall differentiate the behavior of aromatic and aliphatic compounds once contacting a saline solution. Future work will explore the synergetic impact of polar and non-polar hydrocarbons and also, the variation of surface charge at broader salinity ranges.

CRediT authorship contribution statement

Mohammad Hasan Badizad: Conceptualization, Methodology, Software, Investigation, Validation. **Mohammad Mehdi Koleini:** Writing - review & editing. **Remco Hartkamp:** Writing - review & editing. **Shahab Ayatollahi:** Supervision, Project administration. **Mohammad Hossein Ghazanfari:** Supervision.

Declaration of Competing Interest

The authors declare that they have no known competing financial interests or personal relationships that could have appeared to influence the work reported in this paper.

Appendix A. Supplementary material

Supplementary data to this article can be found online at https://doi.org/10.1016/j.jcis.2020.04.060.

References

[1] L. Chong, Y. Lai, M. Gray, Y. Soong, F. Shi, Y. Duan, Effects of frothers and oil at saltwater-air interfaces for oil separation: molecular dynamics simulations and experimental measurements, J. Phys. Chem. B. 121 (2017) 6699–6707, https://doi.org/10.1021/acs.jpcb.7b03313.

[2] A. Dani, G. Keiser, M. Yeganeh, C. Maldarelli, Hydrodynamics of particles at an oil-water interface, Langmuir 31 (2015) 13290–13302, https://doi.org/10.1021/acs.langmuir.5b02146.
[3] H. Guo, A.R. Kovscek, Investigation of the effects of ions on short-range non-DLVO forces at the calcite/brine interface and implications for low salinity oil-recovery processes, J. Colloid Interface Sci. 552 (2019) 295–311, https://doi.org/10.1016/j.jcis.2019.05.049.
[4] P.C. Myint, A. Firoozabadi, Thin liquid films in improved oil recovery from low-salinity brine, Curr. Opin. Colloid Interface Sci. 20 (2015) 105–114, https://doi.org/10.1016/j.cocis.2015.03.002.
[5] M.M. Koleini, M.H. Badizad, Z. Kargozarfard, S. Ayatollahi, The impact of salinity on ionic characteristics of thin brine film wetting carbonate minerals: An atomistic insight, Colloids Surf. A Physicochem. Eng. Asp. 571 (2019) 27–35, https://doi.org/10.1016/j.colsurfa.2019.03.070.
[6] M.M. Koleini, M.H. Badizad, Z. Kargozarfard, S. Ayatollahi, Interactions between rock/brine and oil/brine interfaces within thin brine film wetting carbonates: a molecular dynamics simulation study, Energy Fuels 33 (2019) 7983–7992, https://doi.org/10.1021/acs.energyfuels.9b00496.
[7] M.M. Koleini, M.H. Badizad, M.H. Ghatee, S. Ayatollahi, An atomistic insight into the implications of ion-tuned water injection in wetting preferences of carbonate reservoirs 111530, J. Mol. Liq. 293 (2019), https://doi.org/10.1016/j.molliq.2019.111530.
[8] J.J. Sheng, Critical review of low-salinity waterflooding, J. Pet. Sci. Eng. 120 (2014) 216–224, https://doi.org/10.1016/j.petrol.2014.05.026.
[9] H. Tian, F. Liu, X. Jin, M. Wang, Competitive effects of interfacial interactions on ion-tuned wettability by atomic simulations, J. Colloid Interface Sci. 540 (2019) 495–500, https://doi.org/10.1016/j.jcis.2018.12.108.
[10] D.L. Cheung, Molecular simulation of hydrophobin adsorption at an oil-water interface, Langmuir 28 (2012) 8730–8736, https://doi.org/10.1021/la300777q.
[11] R.I. Slavchov, T.V. Peshkova, Adsorption of ions at the interface oil|aqueous electrolyte and at interfaces with adsorbed alcohol, J. Colloid Interface Sci. 428 (2014) 257–266, https://doi.org/10.1016/j.jcis.2014.04.063.
[12] R. Hartkamp, A.-L. Biance, L. Fu, J.-F. Dufrêche, O. Bonhomme, L. Joly, Measuring surface charge: Why experimental characterization and molecular modeling should be coupled, Curr. Opin. Colloid Interface Sci. 37 (2018) 101–114, https://doi.org/10.1016/j.cocis.2018.08.001.
[13] N. Singh, S. Sharma, H. Vovusha, H. Li, U. Schwingenschlögl, Recent insights from computational materials chemistry into interfaces relevant to enhanced oil recovery, Adv. Theory Simul. 2 (2019) 1800183, https://doi.org/10.1002/adts.201800183.
[14] W.-B. Bartels, H. Mahani, S. Berg, S.M. Hassanizadeh, Literature review of low salinity waterflooding from a length and time scale perspective, Fuel 236 (2019) 338–353, https://doi.org/10.1016/j.fuel.2018.09.018.
[15] F.C.D.A. Lima, R.D.S. Alvim, C.R. Miranda, From single asphaltenes and resins to nanoaggregates: a computational study, Energy Fuels 31 (2017) 11743–11754, https://doi.org/10.1021/acs.energyfuels.7b02002.
[16] G. Hantal, M. Sega, G. Horvai, P. Jedlovszky, Contribution of different molecules and moieties to the surface tension in aqueous surfactant solutions, J. Phys. Chem. C. 123 (2019) 16660–16670, https://doi.org/10.1021/acs.jpcc.9b02553.
[17] T.R. Underwood, H.C. Greenwell, The water-alkane interface at various NaCl salt concentrations: a molecular dynamics study of the readily available force fields, Sci. Rep. 8 (2018) 352, https://doi.org/10.1038/s41598-017-18633-y.
[18] J. Zhao, G. Yao, S.B. Ramisetti, R.B. Hammond, D. Wen, Molecular dynamics simulation of the salinity effect on the n -decane/water/vapor interfacial equilibrium, Energy Fuels 32 (2018) 11080–11092, https://doi.org/10.1021/acs.energyfuels.8b00706.
[19] N.P. Khiabani, A. Bahramian, P. Chen, P. Pourafshary, W.A. Goddard, M.R. Ejtehadi, Calcium chloride adsorption at liquid-liquid interfaces: A molecular dynamics simulation study, Colloids Surf. A Physicochem. Eng. Asp. 527 (2017) 70–80, https://doi.org/10.1016/j.colsurfa.2017.05.019.
[20] E.R. Remesal, J.A. Suárez, A.M. Márquez, J.F. Sanz, C. Rincón, J. Guitián, Molecular dynamics simulations of the role of salinity and temperature on the hydrocarbon/water interfacial tension, Theor. Chem. Acc. 136 (2017) 66, https://doi.org/10.1007/s00214-017-2096-9.
[21] M. Mahmoudvand, A. Javadi, P. Pourafshary, Brine ions impacts on water-oil dynamic interfacial properties considering asphaltene and maltene constituents 123665, Colloids Surf. A Physicochem. Eng. Asp. 579 (2019), https://doi.org/10.1016/j.colsurfa.2019.123665.
[22] Mostafa Lashkarbolooki, Masoud Riazi, Shahab Ayatollahi, Ali Zeinolabedini Hezave, Synergy effects of ions, resin, and asphaltene on interfacial tension of acidic crude oil and low–high salinity brines, Fuel 165 (2016) 75–85, https://doi.org/10.1016/j.fuel.2015.10.030.
[23] M. Bonto, A.A. Eftekhari, H.M. Nick, An overview of the oil-brine interfacial behavior and a new surface complexation model, Sci. Rep. 9 (2019) 6072, https://doi.org/10.1038/s41598-019-42505-2.
[24] T. Austad, S.F. Shariatpanahi, S. Strand, C.J.J. Black, K.J. Webb, Conditions for a low-salinity enhanced oil recovery (EOR) effect in carbonate oil reservoirs, Energy Fuels 26 (2012) 569–575, https://doi.org/10.1021/ef201435g.
[25] M.A. Sohal, G. Thyne, E.G. Søgaard, Review of recovery mechanisms of ionically modified waterflood in carbonate reservoirs, Energy Fuels 30 (2016) 1904–1914, https://doi.org/10.1021/acs.energyfuels.5b02749.
[26] S. Singh, J.D. McLean, P.K. Kilpatrick, Fused ring aromatic solvency in destabilizing water-in-asphaltene-heptane-toluene emulsions, J. Dispers. Sci. Technol. 20 (1999) 279–293, https://doi.org/10.1080/01932699908943792.
[27] J.D. McLean, P.K. Kilpatrick, Effects of asphaltene aggregation in model heptane-toluene mixtures on stability of water-in-oil emulsions, J. Colloid Interface Sci. 196 (1997) 23–34, https://doi.org/10.1006/jcis.1997.5177.
[28] E. Griffiths, Handbook of chemistry and physics a ready-reference pocket book of chemical and physical data, Nature 109 (1922) 369–370, https://doi.org/10.1038/109369a0.
[29] S. Plimpton, P. Crozier, A. Thompson, LAMMPS-large-scale atomic/molecular massively parallel simulator, Sandia Natl. Lab., 2007.
[30] W.L. Jorgensen, J. Chandrasekhar, J.D. Madura, R.W. Impey, M.L. Klein, Comparison of simple potential functions for simulating liquid water, J. Chem. Phys. 79 (1983) 926–935, https://doi.org/10.1063/1.445869.
[31] I.S. Joung, T.E. Cheatham, Determination of alkali and halide monovalent ion parameters for use in explicitly solvated biomolecular simulations, J. Phys. Chem. B. 112 (2008) 9020–9041, https://doi.org/10.1021/jp8001614.
[32] C.D. Williams, P. Carbone, A classical force field for tetrahedral oxyanions developed using hydration properties: The examples of pertechnetate (TcO 4 −) and sulfate (SO 4 2−), J. Chem. Phys. 143 (2015), https://doi.org/10.1063/1.4934964 174502.
[33] M. Hloucha, U.K. Deiters, Fast coding of the minimum image convention, Mol. Simul. 20 (1998) 239–244, https://doi.org/10.1080/08927029808024180.
[34] C. Vega, E. de Miguel, Surface tension of the most popular models of water by using the test-area simulation method 154707, J. Chem. Phys. 126 (2007), https://doi.org/10.1063/1.2715577.
[35] E. Braun, S.M. Moosavi, B. Smit, Anomalous effects of velocity rescaling algorithms: the flying ice cube effect revisited, J. Chem. Theory Comput. 14 (2018) 5262–5272, https://doi.org/10.1021/acs.jctc.8b00446.
[36] A. Grossfield, P.N. Patrone, D.R. Roe, A.J. Schultz, D. Siderius, D.M. Zuckerman, Best practices for quantification of uncertainty and sampling quality in molecular simulations [Article v1.0], Living J. Comput. Mol. Sci. 1 (2019).
[37] J.L. Chen, B. Xue, D.B. Harwood, Q.P. Chen, C.J. Peters, J.I. Siepmann, A Monte Carlo simulation study of the interfacial tension for water/oil mixtures at elevated temperatures and pressures: Water/n-dodecane, water/toluene, and water/(n-dodecane + toluene), Fluid Phase Equilib. 476 (2018) 16–24, https://doi.org/10.1016/j.fluid.2017.06.015.
[38] B. Kumar, Effect of salinity on the interfacial tension of model and crude oil systems, 2012.
[39] M.M. Koleini, M.H. Badizad, S. Ayatollahi, An atomistic insight into interfacial properties of brine nanofilm confined between calcite substrate and hydrocarbon layer, Appl. Surf. Sci. 490 (2019) 89–101, https://doi.org/10.1016/j.apsusc.2019.05.337.
[40] J.-C. Neyt, A. Wender, V. Lachet, A. Ghoufi, P. Malfreyt, Prediction of the concentration dependence of the surface tension and density of salt solutions: atomistic simulations using Drude oscillator polarizable and nonpolarizable models, Phys. Chem. Chem. Phys. 15 (2013) 11679, https://doi.org/10.1039/c3cp50904d.
[41] Mills, Lobo, Self-diffusion in electrolyte solutions: a critical examination of data compiled from the literature, 2013.
[42] R. Mills, A remeasurement of the self-diffusion coefficients of sodium ion in aqueous sodium chloride solutions, J. Am. Chem. Soc. 77 (1955) 6116–6119, https://doi.org/10.1021/ja01628a008.
[43] H. Weingärtner, W.E. Price, A.V.J. Edge, R. Mills, Transport measurements in aqueous sodium sulfate. Evidence for like-ion pairs in concentrated solutions, J. Phys. Chem. (1993).
[44] M. Kunieda, K. Nakaoka, Y. Liang, C.R. Miranda, A. Ueda, S. Takahashi, H. Okabe, T. Matsuoka, Self-accumulation of aromatics at the oil−water interface through weak hydrogen bonding, J. Am. Chem. Soc. 132 (2010) 18281–18286, https://doi.org/10.1021/ja107519d.
[45] M. Kunieda, Y. Liang, Y. Fukunaka, T. Matsuoka, K. Takamura, N. Loahardjo, W. Winoto, N.R. Morrow, Spreading of multi-component oils on water, Energy Fuels 26 (2012) 2736–2741, https://doi.org/10.1021/ef201530k.
[46] M.M. Koleini, M.H. Badizad, R. Hartkamp, S. Ayatollahi, M.H. Ghazanfari, The impact of salinity on the interfacial structuring of an aromatic acid at the calcite/brine interface: an atomistic view on low salinity effect, J. Phys. Chem. B. 124 (2020) 224–233, https://doi.org/10.1021/acs.jpcb.9b06987.
[47] Handbook of Pharmaceutical Salts: Properties, Selection, and Use, Chem. Int. – Newsmag. IUPAC. 24 (2002). https://doi.org/10.1515/ci.2002.24.3.20a.
[48] M.F. Döpke, J. Lützenkirchen, O.A. Moultos, B. Siboulet, J.-F. Dufrêche, J.T. Padding, R. Hartkamp, Preferential adsorption in mixed electrolytes confined by charged amorphous silica, J. Phys. Chem. C. 123 (2019) 16711–16720, https://doi.org/10.1021/acs.jpcc.9b02975.
[49] D.M. Sherman, M.D. Collings, Ion association in concentrated NaCl brines from ambient to supercritical conditions: results from classical molecular dynamics simulations, Geochem. Trans. 3 (2002) 102, https://doi.org/10.1039/b208671a.
[50] H. Wang, E. Carlson, D. Henderson, R.L. Rowley, Molecular dynamics simulation of the liquid–liquid interface for immiscible and partially miscible mixtures, Mol. Simul. 29 (2003) 777–785, https://doi.org/10.1080/0892702031000121842.
[51] S. Paul, A. Chandra, Hydrogen bond dynamics at vapour–water and metal–water interfaces, Chem. Phys. Lett. 386 (2004) 218–224, https://doi.org/10.1016/j.cplett.2003.12.120.
[52] P. Jungwirth, D.J. Tobias, Specific ion effects at the air/water interface, Chem. Rev. 106 (2006) 1259–1281, https://doi.org/10.1021/cr0403741.
[53] T.-M. Chang, L.X. Dang, Recent advances in molecular simulations of ion solvation at liquid interfaces, Chem. Rev. 106 (2006) 1305–1322, https://doi.org/10.1021/cr0403640.

[54] L. Sun, X. Li, Y. Tu, H. Ågren, Origin of ion selectivity at the air/water interface, Phys. Chem. Chem. Phys. 17 (2015) 4311–4318, https://doi.org/10.1039/C4CP03338H.
[55] P. Jungwirth, D.J. Tobias, Ions at the air/water interface, J. Phys. Chem. B. 106 (2002) 6361–6373, https://doi.org/10.1021/jp020242g.
[56] L.F.M. Franco, M. Castier, I.G. Economou, Anisotropic parallel self-diffusion coefficients near the calcite surface: A molecular dynamics study 084702, J. Chem. Phys. 145 (2016), https://doi.org/10.1063/1.4961408.
[57] A.S. Mahadevi, G.N. Sastry, Cation−π interaction: its role and relevance in chemistry, biology, and material science, Chem. Rev. 113 (2013) 2100–2138, https://doi.org/10.1021/cr300222d.
[58] A. Choudhary, A. Chandra, Spatial and orientational structure of the hydration shell of benzene in sub- and supercritical water, J. Phys. Chem. B. 119 (2015) 8600–8612, https://doi.org/10.1021/acs.jpcb.5b03371.
[59] A. Choudhary, A. Chandra, Anisotropic structure and dynamics of the solvation shell of a benzene solute in liquid water from ab initio molecular dynamics simulations, Phys. Chem. Chem. Phys. 18 (2016) 6132–6145, https://doi.org/10.1039/C5CP07352A.
[60] A. Choudhary, A. Chandra, Dynamics of water in conical solvation shells around a benzene solute under different thermodynamic conditions, Phys. Chem. Chem. Phys. 20 (2018) 18328–18339, https://doi.org/10.1039/C7CP08109J.
[61] R.L. Misiorowski, M.A. Wells, Competition between cations and water for binding to phosphatidylcholines in organic solvents, Biochemistry 12 (1973) 967–975, https://doi.org/10.1021/bi00729a028.
[62] Anan Tongraar, Jiraroj T-Thienprasert, Saroj Rujirawat, Sukit Limpijumnong, Structure of the hydrated Ca2+ and Cl−: Combined X-ray absorption measurements and QM/MM MD simulations study, Phys. Chem. Chem. Phys. 12 (36) (2010) 10876, https://doi.org/10.1039/c0cp00136h.
[63] M. Albertí, A. Aguilar, F. Pirani, Cation−π-anion interaction in alkali ion−benzene−halogen ion clusters †, J. Phys. Chem. A. 113 (2009) 14741–14748, https://doi.org/10.1021/jp904852x.
[64] T.C. Dinadayalane, A. Hassan, J. Leszczynski, A theoretical study of cation–π interactions: Li+, Na+, K+, Be2+, Mg2+ and Ca2+ complexation with mono- and bicyclic ring-fused benzene derivatives, in: 2012: pp. 83–93. https://doi.org/10.1007/978-3-642-31750-7_8.
[65] E.A. Orabi, G. Lamoureux, Cation−π and π−π interactions in aqueous solution studied using polarizable potential models, J. Chem. Theory Comput. 8 (2012) 182–193, https://doi.org/10.1021/ct200569x.
[66] A.K. Paul, S. Kolakkandy, W.L. Hase, Dynamics of Na + (benzene) + benzene association and ensuing Na + (benzene) 2 * dissociation, J. Phys. Chem. A. 119 (2015) 7894–7904, https://doi.org/10.1021/acs.jpca.5b01922.
[67] M. Rücker, W.-B. Bartels, G. Garfi, M. Shams, T. Bultreys, M. Boone, S. Pieterse, G.C. Maitland, S. Krevor, V. Cnudde, H. Mahani, S. Berg, A. Georgiadis, P.F. Luckham, Relationship between wetting and capillary pressure in a crude oil/brine/rock system: From nano-scale to core-scale, J. Colloid Interface Sci. 562 (2020) 159–169, https://doi.org/10.1016/j.jcis.2019.11.086.